

RSC Advances



This is an *Accepted Manuscript*, which has been through the Royal Society of Chemistry peer review process and has been accepted for publication.

Accepted Manuscripts are published online shortly after acceptance, before technical editing, formatting and proof reading. Using this free service, authors can make their results available to the community, in citable form, before we publish the edited article. This *Accepted Manuscript* will be replaced by the edited, formatted and paginated article as soon as this is available.

You can find more information about *Accepted Manuscripts* in the [Information for Authors](#).

Please note that technical editing may introduce minor changes to the text and/or graphics, which may alter content. The journal's standard [Terms & Conditions](#) and the [Ethical guidelines](#) still apply. In no event shall the Royal Society of Chemistry be held responsible for any errors or omissions in this *Accepted Manuscript* or any consequences arising from the use of any information it contains.

Properties of indium doped nanocrystalline ZnO thin films and their enhanced gas sensing performance

Sumati Pati*, P. Banerji and S. B. Majumder

Materials Science Centre, Indian Institute of Technology, Kharagpur-721302

RSC Advances Accepted Manuscript

Key words: Thin film; Indium doping; Hall measurement; Gas sensor

* Corresponding author. Mobile: +91 9438855121; Email: sumatipati.11@gmail.com

Abstract

Zinc oxide (ZnO) is one of the most promising semiconducting metal oxides, particularly for gas sensing application. Impurity doped ZnO has offered much improved sensing performance, as compared to its undoped counterpart. In this work, undoped as well as indium doped nanocrystalline ZnO thin films are synthesized by a low cost chemical solution deposition route. X-ray diffraction pattern of the synthesized films reveal preferential orientation along the (002) plane. The surface and cross section morphology has clearly changed with the variation of indium content. Optical transmittance values are sensibly increased with increase in indium concentration and the band gap energy is found in the range 3.210 eV-3.221 eV. PL spectra reveal three characteristic peaks, owing to band to band transition and defect level emissions. The effect of indium doping on the electrical parameters of ZnO are analyzed through Hall effect measurement at room temperature. The gas sensing characteristics of these sensors offer good reproducibility and stability towards various reducing gases, with an enhancement of response% and lower detection limit as compared to undoped ZnO. A doping level of 3 wt% of indium in ZnO is found to give optimum response and a lowest detection limit of 1 ppm or even less amount of hydrogen. However, further increase in doping concentration resulted in reducing the sensing parameters. This is attributed to the gas sensing mechanism related to the substitution of In^{3+} ions at Zn^{2+} ion sites thus enhancing the free charge carriers at the optimum level of indium. Exploring this gas sensing mechanism, it is argued that the sensor performance can be dramatically improved by tailoring the indium concentration in ZnO for its practical application in various sectors as an effective gas sensor.

1. Introduction

ZnO is an attractive material for gas sensor [1-3], owing to its abundance in nature, non toxicity, low cost, and so on. Though it can be synthesized in different forms such as thin film [4], thick film [5], pellets [6], etc., thin film form is more effective due to its small size, low consumption of source materials, and large surface to volume ratio, low power consumption, feasibility in integrated circuits and more specifically for its improved gas sensing performance. Since the gas sensing mechanism in these thin films involve surface oxidation, electron exchange and desorption of the reaction products, the measured resistance transients during response and recovery depends on a variety of factors interrelated to each other. For example, the response is related to the concentration of intrinsic carriers and their mobility. The intrinsic carrier concentration can be modified by aliovalent doping which in turn control the response characteristics of the deposited films. For example, the concentration of the carriers can be significantly improved by doping the ZnO with higher valence elements, such as Al, In and Ga. Theoretical studies demonstrate that as the radii of these dopants are comparable to that of the Zn, they could replace the Zn atoms substitutionally [7-8]. While replacing Zn atom the dopant use only two of its three valence electrons and donates the third electron to the oxide, thus introducing shallow donor levels in the oxide and thus increasing its conductivity. Moreover, out of all the dopants of group III elements indium is considered as one of the most efficient dopant used to enhance the conductivity of ZnO thin films [9]. A number of literatures reported the enhancement of sensing performance of doped ZnO on exposure to various toxic and combustible gases and hydrocarbons [10-22]. Sahay and Nath [10] observed that compared to the undoped ZnO film, Al-doped films (0.5 at% Al-doped ZnO) show higher sensitivity to methanol vapor. It shows the maximum response of ~44% at 275°C to 500 ppm of methanol vapor in air.

Ferro et al. [11] reported that by adding 3 wt% of indium nitrate to the spraying solution it is possible to enhance the film–gas response to 5 ppm of NO₂ at 275°C. Maldonado et al. [12] doped ZnO thin film with fluorine and aluminum and studied the gas sensing performance at different concentrations of CO. They found an optimum response of 93% at 200°C for 200 ppm of CO gas. Sivalingam et al. [13] studied the trimethylamine (TMA) and ethanol vapor sensing performance of manganese doped ZnO thin films. They observed a better sensing response of 300 at 75 ppm of TMA at 373 K. Badadhe and Mulla [21] studied the gas sensing performance of 3 % indium doped ZnO thin film in presence of various gases such as Ethanol, LPG, ammonia, H₂, CO, Nitric oxide and H₂S. They observed highest response of 13,000 towards 1000 ppm of gas at 250°C, however, a response of only 11 and 1.5 towards H₂ and CO gas respectively in the same environment. Thus, from the literature reports the enhancement in sensing performance is ensured by doping ZnO with various impurities. However, to the best of our knowledge very limited attempt has so far been made to understand the effect of various parameters to improve the gas sensing characteristics of indium doped ZnO thin films in presence of toxic and combustible gases.

In the present work, therefore, we have synthesized undoped as well as indium doped ZnO [Zn_{1-x}In_xO (0.0 ≤ x ≤ 0.10)] thin films using a cost effective chemical solution deposition technique. The synthesized films are characterized in terms of their phase purity, microstructure evolution, optical and electrical characteristics. The effect of indium doping on the gas sensing characteristics of ZnO thin film gas sensors on exposure to different reducing gases is investigated. The possible sensing mechanism based on the substitution of In³⁺ ions at Zn²⁺ ion sites and its role in enhancing the gas sensing parameters is analyzed.

2. Experimental details

Zinc acetate dihydrate (purity 98%) and indium nitrate dihydrate (purity 99.99%) powders were first mixed with different molar ratios to prepare 1 wt%, 3 wt%, 5 wt% and 10 wt% indium doped ZnO thin films. The powders were then dissolved in a mixture of 2-methoxyethanol and MEA (monoethanolamine) solution at room temperature separately. The solutions were stirred at 60 °C for 2h to yield their clear and homogeneous form. The concentrations of the solutions were kept at ~ 0.4 M. The solutions were then spin cast onto quartz substrates using a spin coater unit (SCU 2007, apex instruments co.) which was rotated at 3000 rpm for 30 s. After deposition, the films were heat treated at 300°C for 5 min to evaporate the solvent and to remove the organic residuals. The coating and subsequent heating was repeated to yield the films. The films were finally annealed at 600°C for 1 h in air.

The phase formation behavior of the prepared ZnO thin films was studied by X-ray diffraction (Ultima III, Rigaku, Japan) analyses. In the present study the X-ray diffraction patterns are recorded using CuK_α radiation in 2θ range 20-80 degree at a scanning rate 3 degree min^{-1} . During the operation of the instrument, the accelerating voltage and current is kept 40 kV and 30 mA respectively. The micro structural characteristics of the films were investigated using field emission scanning electron microscope (FESEM) (SUPRA-40, Carl Zeiss, Germany). The optical properties of the synthesized films were investigated by analyzing the transmission and absorption spectra recorded in ultraviolet-visible (UV-VIS) range using UV-VIS absorption spectrometer (Lambda 750, Perkin Elmer, USA). The room temperature photoluminescence (PL) spectra of these films were recorded using He–Cd laser as an excitation source, operating at 325 nm with an output power of 45 mW and a TRIAX 320 monochromator fitted with a cooled Hamamatsu R928 photomultiplier detector. Electrical characteristics of the grown films are

studied by high temperature Hall effect measurement using four probe techniques. For the measurement of gas sensing characteristics of ZnO thin films the surface of the film was coated with gold electrodes. The gas sensing performance was evaluated using an automated dynamic volume measurement set-up developed in our laboratory. The reactor chamber is equipped with several mass flow controllers and gas-mixing chamber for accurate control of test gas concentration. An electrometer interfaced with a PC (through Labview software and GPIB interface) was used to measure the resistance change upon exposing the sensor to various reducing gases. The detail of the measurement set up is described elsewhere [23].

3. Results and discussion

3.1. Structural characterization

Fig. 1 (a) shows the XRD patterns of the ZnO thin films, of various indium content [$\text{Zn}_{1-x}\text{In}_x\text{O}$ ($0.0 \leq x \leq 0.10$)], grown on quartz substrates by chemical solution deposition route. As envisaged from the figure the synthesized films are crystallized into hexagonal wurtzite structure and are textured along (002) plane. The presence of peak only along (002) plane and its reflection along (004) indicates that the grown films are textured along c-axis, i.e. perpendicular to the substrates. The underlying mechanism that controls the preferential growth of these films along (002) plane is not very well understood. However, since the wurtzite structure has minimum surface energy and the highest atomic density of Zn atom along (002) plane, growth along this plane is predominant [24-25]. Presence of only one peak along (002) plane in all the films reflects the uniformity in the phase formation behavior of the materials, where there is no additional phase for indium. This confirms that indium substitutes zinc atom without forming any impurity phase. The XRD pattern of the undoped ZnO [$\text{Zn}_{1-x}\text{In}_x\text{O}$ ($x = 0$)] thin film shows a highly intense (002) reflection peak and a small peak along (004) plane. However, this pattern

for indium doped ZnO thin films shows peak only along (002) plane (but with diminishing intensity with the increasing wt% of indium), which finally almost disappears for ZnO [$Zn_{1-x}In_xO$ ($x = 10$)] thin film. This behavior was also reported by many researchers [26-27]. It suggests that formation of hexagonal phase in ZnO is hindered by incorporation of more amount of indium into ZnO lattice, thus suppressing the crystalline behavior of the grown films. Moreover, with the increase in indium content the full width at half maximum (FWHM) of the diffraction peaks becomes broad and the position of the (002) peak shifts towards low angle as shown in the Fig. 1 (b). Noting systematic shift of (002) diffraction peak with the increase of indium contents we confirmed the inclusion of indium in ZnO lattice. This behavior may be attributed to the distortion in ZnO lattice due to the substitution of Zn^{2+} by In^{3+} ions. As the atomic radii of the In^{3+} ion ($r = 0.080$ nm) is more than that of Zn^{2+} ($r = 0.074$ nm), it causes a distortion in the ZnO lattice causing a shifting of (002) peak position towards low angle and also a broadening of XRD pattern [26-27]. This indicates that an increase in doping concentration deteriorates the crystallinity of films, which may be the consequence of the stress developed due to the difference in size between Zn^{2+} and In^{3+} ions [28].

The crystallite size (D) of the synthesized films is estimated using the Debye-Scherrer formula [29]:

$$D = 0.9 \lambda / \beta \cos \theta \quad (1)$$

Where λ ($= 0.154$ nm) is the wavelength of the X-ray radiation used, θ is the angle of incidence and β is the full width at half maximum (FWHM) of diffraction peaks measured in radian. The inter planar spacing (d_{hkl}) can be determined using Bragg equation $2d_{hkl} \sin \theta = n\lambda$. Where 'n' is

the order of diffraction, hkl the Miller indices of the plane of diffraction. For the hexagonal lattice, d_{hkl} can be written as

$$\frac{1}{d_{hkl}^2} = \frac{4}{3} \left(\frac{h^2 + k^2 + hk}{a^2} \right) + \frac{l^2}{c^2} \quad (2)$$

Where a and c are the lattice parameters for the hexagonal phase. In Eq. (2), putting $hkl = 002$, parameters for the hexagonal ZnO thin films are estimated. The calculated lattice parameters, and d_{hkl} values of all the grown ZnO thin films are tabulated in Table-1. As discussed, shifting of peak position towards low angle and broadening of the XRD peak, decrease of crystallite size and increase of lattice strain with the increase in indium content is reflected from the table.

3.2. Microstructure

Fig. 2 (a-e) shows the surface morphology of indium doped ZnO thin films with various indium contents (a) 0 wt%, (b) 1 wt%, (c) 3 wt%, (d) 5 wt% and (e) 10 wt%. Their cross sectional morphologies are shown in Fig. 2f-2g respectively.

The grain size appears to decrease with increase in indium concentration from 1 wt% to 10 wt%. This confirms the role of substitutional dopant in deterioration of the degree of crystallization of the films. The same trend in the change in surface morphology was also reported by Lucio-Lopez et al. [30]. This is also clearly understood from the XRD spectra, where the intensity of (002) peak decreases with increasing indium concentration. For minimum indium content (1 wt%) ZnO thin film, there found some granular structures, whereas the microstructure becomes smoother and more compact with increasing indium concentrations. This reveals the substitution of zinc atoms by indium and also orderly arrangement of indium atoms inside ZnO lattice with increasing indium concentration. As envisaged from the cross-

sectional morphologies, in Fig. 2f-2j, there is no significant change in the thickness of the undoped and indium doped ZnO films, all being in the range (300-400) nm. Undoped ZnO thin film seems to consist of two layers, which is also reported by Lee et al. [31], whereas for 3 wt% and 5 wt% indium concentration there are small spherical grains grown on the top of the substrates. However, further increasing indium concentration leads more and more compact structures.

3.3. Optical characterization

The optical properties of the synthesized films are investigated by analyzing the transmission and absorption spectra recorded in ultraviolet-visible (UV-VIS) range. From the recorded absorption spectra, the values of band gap energy (E_g) of the synthesized films are estimated. Fig. 3 (a) shows the optical transmission spectra of the synthesized films in the wavelength (λ) range 200 – 800 nm. From the figure it is observed that the average optical transmittance of undoped ZnO thin film in the visible range is about 68%, whereas doping with indium dramatically improves this value up to 99% (for 10 wt% of indium). As explained by Chen et al. [32] this is attributed to the reduction in surface roughness with increasing dopant concentration in the ZnO thin films. Reduction in surface roughness reduces the optical scattering thus improving the transmittance of the films. This suppression of crystallinity and reduction of surface roughness with increasing indium concentration, as envisaged from the XRD and FESEM results respectively, improves the optical quality.

From the recorded absorption spectra, it is found that the films have a low absorption in the visible range and a high absorption in the ultra-violet range. This high absorption in the UV range is related to the fundamental absorption and involves the transition of electrons from the

valence to the conduction band, which can be used to determine the band gap energy of the semiconductor (ZnO in the present study). The estimated optical band gap energy of the ZnO thin films is shown in the Tauc plot in Fig. 3 (b). The band gap energy (E_g) is determined by extrapolation of the linear portion of $(\alpha hv)^2$ versus hv plots at $\alpha^2 = 0$ using the following equation [33].

$$\alpha hv = A'(hv - E_g)^n \quad (3)$$

Where α is absorption coefficient, hv is the photon energy, E_g the optical band gap energy and A' is a constant. In case of allowed direct transitions, as like in ZnO, the value of n is equal to $\frac{1}{2}$. The intercepts of these plots on the energy axis denotes the energy band gaps, since $E_g = hv$ when $(\alpha hv)^2 = 0$. The measured energy band gap values are in the range of 3.210–3.221 eV, which is close to the band gap of intrinsic ZnO semiconductor and are in good agreement with the literature reports. For undoped ZnO thin film the value of E_g is found to be 3.210 eV, whereas it shifts slightly from 3.215 eV to 3.221 eV with increasing indium concentration from 1 to 10 wt%. This shift of the band gap with indium concentration in ZnO thin films may be related to the concentration of majority carriers, which is also investigated from the study of photoluminescence spectroscopy and Hall effect measurement.

Photoluminescence spectroscopy is a non-destructive technique used to find the defect structures in ZnO thin films. Oxygen vacancies (V_O) and zinc interstitials (Zn_i) are the common donor type defects exist in ZnO [34]. The concentrations of these defects are known to vary significantly by doping it with higher-valence impurities. Fig. 4 shows the room temperature PL spectra of the films recorded using He–Cd laser as an excitation source operating at 325 nm. The excitation energy (~ 3.81 eV) has been chosen to be higher than the band-gap energy of ZnO (3.3

eV) in order to understand the defect emission. The spectra consist of three peaks at about ~389 nm, ~435 nm and ~545 nm. The peak at 389 nm (UV luminescence) is attributed to near band edge (NBE) emission, whereas the other peak ~ 435 nm is attributed to zinc vacancy (V_{Zn}) related emission and the broad peak at ~545 nm (green luminescence) is due to the defect level (DL) emission, primarily oxygen vacancy (V_O), of the synthesized films [35]. PL spectrum of undoped ZnO film is dominated by DL emission primarily V_O , whereas, with the increase of indium concentration PL peak related to zinc vacancy (V_{Zn}) is identified along with the peak corresponding to V_O . Inclusions of In^{3+} into Zn^{2+} indeed induce zinc vacancies to maintain the charge neutrality. In addition, there is a variation of intensity of peaks with the increase in indium concentration, which may be due to the presence of non-radiative traps and defect centers produced due to structural disorder [36]. Further, the spectra are associated with a shifting in peak position, which can again be attributed to the difference in band gap value with different indium contents. XRD pattern, FESEM images and UV-Visible spectroscopy in conjunction with PL spectra suggests that doping ZnO with higher valence impurities reduces crystallization and enhances the defect concentration which may be useful for gas sensing application of these materials.

3.4. Electrical characterization

The electrical properties of the grown ZnO thin films of various indium concentrations [$Zn_{1-x}In_xO$ ($0.0 \leq x \leq 0.10$)] are studied by Hall effect measurement using the Van der Pauw geometry, making ohmic contacts on the samples by thermal evaporation technique. It is found that, indium doping markedly improved the carrier concentration and conductivity, and also indicated *n*-type behavior for all the grown films. Fig. 5 (a) shows the plot of carrier concentration, electron mobility and resistivity at room temperature (RT) for ZnO thin films of

various indium contents. The lowest carrier concentration obtained for the undoped ZnO thin film is $1.32 \times 10^{18} \text{ cm}^{-3}$. The mobility of this sample is approximately $4.89 \text{ cm}^2/\text{Vs}$. The highest carrier concentration of $1.95 \times 10^{19} \text{ cm}^{-3}$ and electron mobility of approximately $2.95 \text{ cm}^2/\text{Vs}$ is obtained for 5 wt% indium doped ZnO thin film. However, with further increase in doping concentration the carrier concentration and mobility decreases to $1.38 \times 10^{19} \text{ cm}^{-3}$ and $2.68 \text{ cm}^2/\text{Vs}$ respectively. It is known that carrier concentration is mainly dependent upon the free carriers available in the material, while Hall mobility is generally affected by the scattering mechanism. A good number of research reports in support of this dependence are available in the literature [37-38]. It is well known that ZnO is intrinsically *n*-type owing to donor defects such as oxygen vacancies and zinc interstitials [34]. In addition, as indium is 3+ valence so its substitution in ZnO lattice, is presumed to enhance the free carrier concentration and hence conductivity of the sample. However, the decrease in carrier concentration for higher doping may be attributed to the higher resistivity of the material.

Hall mobility is an indicator of how well an electron or hole will drift through the semiconductor and is a function of the scattering within the semiconductor. Two prominent scattering mechanisms are lattice scattering and impurity scattering. Lattice scattering, also known as phonon scattering, occurs as atoms in a semiconductor contain a certain amount of thermal energy, causing atoms to vibrate around their equilibrium lattice sites. These lattice vibrations result in phonons (quantized lattice vibrations) displaying different energies. Since this scattering mechanism is a function of the thermal motion of atoms, the mobility is a strong function of temperature. Mobility decreases as temperature increases. This is dominant in undoped ZnO thin films; however the impurity scattering dominates in doped ZnO thin films. Impurity scattering occurs as donor and acceptor impurities are ionized and hence a coulomb

interaction occurs between the charged impurities and electrons and holes. When carriers drift into the vicinity of a charged impurity atom, they are deflected or scattered. Mobility decreases as the impurity concentration increases [39-40].

The electronic conductivity of the grown films increases with the increase of carrier concentrations [41]. Fig. 5 also revealed the decrease in resistivity up to 5 wt% of indium doped ZnO thin film is owing to the increase in carrier concentration and the increase in resistivity for higher indium doping (10 wt% of indium) is the consequence of its lower carrier concentration. Many researchers reported similar trend in carrier concentration [42-45], however, the optimum indium concentration (corresponding to highest carrier concentration) is reported to be different in different works.

3.5. Gas sensing characteristics

The gas sensing characteristics of the grown thin films of varying indium concentrations are investigated in presence of various reducing gases, such as carbon monoxide (CO), hydrogen (H₂) and methane (CH₄). The mechanism of these reducing gas sensing characteristics of 'n' type semi-conducting oxide thin film gas sensor is well explained in the literature [46-47]. When these sensors are heated at higher temperature, depending on the surface temperature various forms of oxygen from the atmosphere are adsorbed on the surface of the thin film. Moreover, in the present study In³⁺ cation enhances the adsorption of these oxygen ions. Indium (In³⁺) being trivalent, to maintain the charge neutrality in ZnO lattice it creates excess lattice oxygen vacancy. This facilitates the surface adsorption of oxygen ions. These adsorbed oxygen attract electron from the conduction band of metal oxide, thus increasing the space-charge layer thickness. This impedes motion of electrons between adjacent grains and hence the sensor resistance increases.

This sensor resistance (R_a) becomes stable in air with the saturation of adsorbed oxygen. Now exposure of reducing gases to the sensor surface releases back the conduction electrons to the metal oxide thereby decreasing the sensor resistance. This sensor resistance (R_g) attains saturation with time. The response (S) of the sensor is determined by the following relation [46],

$$s = \left(\frac{R_a - R_g}{R_a} \right) \times 100 \quad (4)$$

Fig. 6 shows a typical resistance transient plot recorded for 3 wt% indium doped ZnO thin film gas sensor towards hydrogen gas detection at an operating temperature $\sim 350^\circ\text{C}$, optimum temperature for hydrogen gas in the present study. As observed the sensor exhibits well reproducibility with a very minimal base line drift. In a similar way, the resistance transients for the all the gas sensors are recorded at different operating temperatures, in presence of all the mentioned gases and the response% are calculated from the measured resistance transients using the Eq. 4. Fig. 7 (a-c) represents the variation of response% of all the sensors as a function of operating temperatures for three different gases at a fixed gas concentration (~ 1660 ppm). Note that, for all the sensors the response% increases with increase in operating temperature and have an optimum temperature (T_{opt} , corresponding to the maximum response) 350°C , above which it reduces. Similar results (existence of optimum operating temperature) have also been reported for a variety of SMO sensors [48-49]. Such behavior can be explained using the concept of activation energy. At a lower temperature the reducing gas molecules may not acquire enough energy to react with the adsorbed oxygen species. However, at higher temperature the acquired energy may be sufficient to meet the activation energy of the reaction and hence the reaction rate increases with concomitant increase in the response. While the reduction of response at still higher temperature (beyond optimum temperature) could be due to the enhancement of

desorption rates of the surface adsorbed oxygen species. Fig. 7 (d) shows a typical comparison plot representing the enhancement of response% of ZnO thin film when doped with indium.

Fig. 8 shows the resistance transients of 3 wt% indium doped ZnO thin films during response and recovery of hydrogen gas sensing at operating temperature $\sim 300^\circ\text{C}$. Using Eq. 4 the response% is estimated and is marked in the figure against each concentration separately. It is observed that with increase in gas concentration response% increases. Note that this sensor can detect up to 1 ppm or even less amount of hydrogen, which is very effective for its use as a hydrogen gas sensor. Response% of all the sensors in presence of various concentrations of different gases (hydrogen, carbon monoxide and methane) is also recorded and is plotted in Fig. 9. In Table 2 we have compared the gas sensing performance of our indium doped ZnO film with other impurity doped sensors reported in the literature. Comparing the sensing performance we can state that our sensor can have a very good stand in the existing literature. Reviewing Fig. 9 a linear variation of response% with test gas concentration (C_{gas}) in accordance with the relationship [50]:

$$\text{Response\%} = AC_{\text{gas}}^n \quad (5)$$

is observed, where A and n are constants. It is also observed that this rate of variation in gas concentration is different for different gases and also varies from lower to higher gas concentration. However, further study will be beneficial in explaining the concentration dependent change in response% of this indium doped ZnO thin film gas sensors. Reviewing the microstructure, PL spectroscopy and Hall effect measurement, it is found that all the observed results are in well agreement with the enhancement in sensing performance for optimum indium doped ZnO thin film.

4. Conclusion

We have synthesized submicron (< 500 nm) $\text{Zn}_{1-x}\text{In}_x\text{O}$ ($0.0 \leq x \leq 0.10$) thin films by chemical solution deposition technique. The synthesized films are crystallized into hexagonal wurtzite structure and are textured along (002) plane. Noting systematic shift of (002) diffraction peaks with the increase of indium doping contents we confirmed the inclusion of indium in ZnO lattice. The crystallite size (in the range of 8 to 45 nm) is found to decrease with concomitant increase of lattice strain with the increase of indium concentration. The thickness of indium doped ZnO films are in the range of 300 – 400 nm. PL spectra of undoped ZnO films are dominated by oxygen vacancies ($V_{\text{O}}^{\bullet\bullet}$). However, with the increase of indium concentration PL peak related to zinc vacancy (V_{Zn}^{\bullet}) is also identified along with the peak correspond to $V_{\text{O}}^{\bullet\bullet}$. Inclusions of In^{3+} into Zn^{2+} indeed induce zinc vacancies to maintain the charge neutrality. The carrier concentration is increased in indium doped ZnO with systematic reduction of resistivity with indium doping concentration up to 5 wt% in ZnO. The response% and stability of indium doped ZnO thin films were evaluated for various combustible gases by varying the operating temperature and gas concentration. Optimal indium doping is found to markedly improve the response% of combustible gas sensing in conjunction with faster response kinetics, as compared to its undoped counterpart. Studying gas sensing characteristics, it is demonstrated that the gas solid interaction is influenced by the dopant induced point defects, change in morphology as well as kinetics of gas diffusion through porosity.

References

1. C. Wang, L. Yin, L. Zhang, D. Xiang and R. Gao, *Sensors* 2010, **10**, 2088.
2. D. E. Williams, *Sens. Actuators B* 1999, **57**, 1.
3. N. Barsan, D. Koziej and U. Weimar, *Sens. Actuators B* 2007, **121**, 18.

4. H. Cheng, C. Chen and C. Tsay, *Appl. Phys. Lett.* 2007, **90**, 012113 (1).
5. R. Y. Borse and V. T. Salunke, *Sens. Transduc. J.* 2010, **9**, 161.
6. P. P. Sahay, S. Tewari, R. K. Nath, S. Jha and M. Shamsuddin, *J. Mater. Sci.* 2008, **43**, 4534.
7. H. Metiu, S. Chretien, Z. Hu, B. Li and X. Y. Sun, *J. Phys. Chem. C* 2012, **116**, 10439.
8. V. Khranovskyy, U. Grossner, O. Nilsen, V. Lazorenko, G.V. Lashkarev, B.G. Svensson and R. Yakimova, *Thin Solid Films* 2006, **515**, 472.
9. L. Xu, Y. Su, Y. Chen, H. Xiao, L. Zhu, Q. Zhou and S. Li, *J. Phys. Chem. B* 2006, **110**, 6637.
10. P.P. Sahay and R.K. Nath, *Sens. Actuators B* 2008, **134**, 654.
11. R. Ferro, J.A. Rodríguez and P. Bertrand, *Thin Solid Films* 2008, **516**, 2225.
12. A. Maldonado, S. Tirado-Guerra, J.M. Cázares and M. de la L. Olvera, *Thin Solid Films* 2010, **518**, 1815.
13. D. Sivalingam, J. B. Gopalakrishnan and J. B. B. Rayappan, *Sens. Actuators B* 2012, **166**, 624.
14. C. S. Prajapati and P. P. Sahay, *Mater. Sci. Semicon. Proc.* 2013, **16**, 200.
15. N. H. Al-Hardan, M.J. Abdullah and A. A. Aziz, *Appl. Surf. Sci.* 2013, **270**, 480.
16. A. Ghosh, A. Ghule and R. Sharma, *J. Phys.: Conference Series* 2012, 365, 012022 (4).
17. R. K. Nath, S. S. Nath and K. Sunar, *J. Anal. Sci. Tech.* 2012, **3**, 85.
18. N. Kilinc, S. Ozturk, L. Arda, A. Altinadal and Z. Z. Ozturk 2012, *J. Alloy Compd.*, **536**, 138.
19. T. T. Trinh, N. H. Tu, H. H. Le, K. Y. Ryu, K. B. Le, K. Pillai and J. Yi 2011, *Sens. Actuators B*, **152**, 73.

20. Y. Liu, T. Hang, Y. Xie, Z. Bao, J. Song, H. Zhang and E. Xie 2011, *Sens. Actuators B*, **160**, 266.
21. S. S. Badadhe and I.S. Mulla 2009, *Sens. Actuators B*, **143**, 164.
22. G.-H. Kuo, H. P. Wang, H. H. Hsu, J. Wang, Y. M. Chiu, C.-J. G. Jou, T. F. Hsu and F.-L. Chen 2009, *J. Nanomater.*, **2009**, 316035(3).
23. K. Mukherjee and S.B. Majumder, *J. Appl. Phys.* 2009, **106**, 064912 (1).
24. S. Amirhaghi, V. Craciun, D. Craciun, J. Elder and I. W. Boyd, *Microelectron. Engg.* 1994, **25**, 32 l.
25. D. Bao, H. Gu and A. Kuang, *Thin Solid Films* 1998, **312**, 37.
26. S. Y. Bae, C. W. Na, J. H. Kang and J. Park, *J. Phys. Chem. B* 2005, **109**, 2526.
27. A. E. Morales, M. H. Zaldivar and U. Pal, *Opt. Mater.* 2006, **29**, 100.
28. J. Nishino, S. Ohshio and K. Kamata, *J. Am. Ceram. Soc.* 1992, **75**, 3469.
29. Cullity, B. D. (2001), *Elements of x-ray diffraction*, 3rd ED. Prentice Hall, New York.
30. M.A. Lucio-Lopez, M.A. Luna-Arias, A. Maldonado, M. de la L. Olvera and D.R. Acosta, *Sol. Energ. Mat. Sol. C.* 2006, **90**, 733.
31. J.-H. Lee and B.-O. Park, *Thin Solid Films* 2003, **426**, 94.
32. K. J. Chen, F. Y. Hung, Y. T. Chen, S. J. Chang and Z. S. Hu, *Mater. Transactions* 2010, **51**, 1340.
33. A. K. Chawla, D. Kaur and R. Chandra, *Opt. Mater.* 2007, **29**, 995.
34. A. Janotti and C. G Van de Walle, *Rep. Prog. Phys.* 2009, **72**, 126501 (29).
35. N. K. Singh, S. Shrivastava, S. Rath and S. Annapoorni, *Appl. Surf. Sci.* 2010, **257**, 1544.

36. P. M. R. Kumar, C S. Kartha, K. P. Vijayakumar, T. Abe, Y. Kashiwaba, F. Singh and D. K. Avasthi, *Semicond. Sci. Tech.* 2005, **20**, 120.
37. C.-J. Xian, J.-K. Ahn, N.-J. Seong, S.-G. Yoon, K.-H. Jang and W.-H. Park, *J. Phys. D: Appl. Phys.* 2008, **41**, 215107 (5).
38. J. Mass, P. Bhattacharya and R.S. Katiyar, *Mater. Sci. Engg. B* 2003, **103**, 9.
39. T Minami, *Mater. Res. Bull.* 2000, **25**, 38.
40. R. B. H. Tahar, *J. Eur. Ceram. Soc.* 2005, **25**, 3301.
41. P. Banerjee, W.-J. Lee, K.-R. Bae, S. B. Lee and G. W. Rubloff, *J. Appl. Phys.* 2010, **108**, 043504 (7).
42. H. Khallaf, G. Chai, O. Lupan, L. Chow, S Park and A. Schulte, *J. Phys. D: Appl. Phys.* 2008, **41**, 185304.
43. A. Hafdallah, F. Yanineb, M.S. Aida and N. Attaf, *J. Alloy Compd.* 2011, **509**, 7267.
44. D. H. Kim, N. G. Cho, H. G. Kim and W.-Y. Choi, *J. Electrochem. Soc.* 2007, **154**, 939.
45. C.E. Benouis, M. Benhaliliba, A. S. Juarez, M.S. Aida, F. Chami and F. Yakuphanoglu, *J. Alloy Compd.* 2010, **490**, 62.
46. S. Pati, S.B. Majumder and P. Banerji, *J. Alloy Compd.* 2012, **541**, 376.
47. S. Shukla, S. Seal, L. Ludwig and C. Parish, *Sens. Actuators B* 2004, **97**, 256.
48. H. Zhao, Y. Li, L. Yang and X. Wu, *Mater. Chem. Phys.* 2008, **112**, 244.
49. C. Aifan, H. Xiaodong, T. Zhangfa, B. Shouli, L. Ruixian and L.C. Chiun, *Sens. Actuators B* 2006, **115**, 316.
50. S. Pati, A. Maity, P. Banerji and S.B. Majumder, *Analyst* 2014, **139**, 1796.

Figure captions

Fig. 1: (a) XRD pattern of (a) undoped ZnO (b) ZnO: In 1 wt% (c) ZnO: In 3 wt% (d) ZnO: In 5 wt%, and (e) ZnO: In 10 wt% thin films. Inset shows the magnified image of (002) peaks of the corresponding films. Fig. 1(b) Position of the (002) peak and full width at half-maxima (FWHM), obtained from the XRD pattern of undoped and indium doped ZnO thin films

Fig. 2: Scanning electron micrographs of indium doped ZnO thin films of various indium concentration: (a) 0 wt%, (b) 1 wt%, (c) 3 wt%, (d) 5 wt% and (e) 10 wt% and their cross sectional morphology are shown, in the right hand side of the respective films, in Fig. 2f-2j

Fig. 3: (a) Transmission spectra and (b) Tauc plot (showing the band gap of the material) of (a) undoped ZnO, (b) ZnO: In 1 wt%, (c) ZnO: In 3 wt%, (d) ZnO: In 5 wt% and (e) ZnO: In 10 wt% thin films in the wavelength range 250 – 800 nm

Fig. 4: PL spectra of (a) undoped ZnO, (b) ZnO: In 1 wt%, (c) ZnO: In 3 wt%, (d) ZnO: In 5 wt%, and (e) ZnO: In 10 wt% thin films using He-Cd laser source at an excitation wavelength of 325 nm

Fig. 5: Plot showing the variation of carrier concentration, mobility and resistivity of the ZnO thin films of various indium concentration at room temperature

Fig. 6: Resistance transients recorded for 3 wt% indium doped ZnO thin film sensing element towards the detection of 1660 ppm of hydrogen gas at its optimum temperature

Fig. 7: Variation of response% of ZnO thin film gas sensors (of various indium concentration) towards the detection of 1660 ppm of (a) H₂, (b) CO and (c) CH₄ gas as a function of operating temperature, (d) Comparison of gas sensing performance of undoped and 3 wt% indium doped ZnO thin film at different operating temperatures

Fig. 8: The time dependent hydrogen gas response of 3 wt% indium doped ZnO thin film gas sensor measured at 350°C, varying the hydrogen concentration in the range of (1660-1) ppm

Fig. 9: Variation of response% of indium doped ZnO thin film gas sensors towards the detection of various concentrations of (a) H₂, (b) CO and (c) CH₄ gas at their optimum temperature, 350°C

Table-1: Structural parameters of indium doped ZnO thin films, estimated from X-ray diffraction pattern

Indium content (wt%)	Peak position 2θ (degree)	$d_{(002)}$ (Å)	Lattice parameter, c (Å)	FWHM	Crystallite size (nm)	Lattice strain (%)
0	34.913	2.569	5.138	0.196	46.5	0.272
1	34.835	2.573	5.146	0.280	31.8	0.385
3	34.807	2.575	5.150	0.600	14.3	0.835
5	34.802	2.576	5.152	0.720	11.9	1.002
10	34.779	-	-	1.012	8.4	1.618

Table-2: Recent literature reports on gas sensing performance of ZnO thin films doped with various impurities

Dopants	Optimum dopant conc.	Gas type	Gas conc.(ppm)	T _{opt} (°C)	Response		Ref.
					R _a /R _g	ΔR/R _a	
Al	0.5 at%	methanol	500	275	-	44	[10]
In	3 at%	NO ₂	5	275	~54	-	[11]
F, Al		CO	200	200		93	[12]
Mn	0.004M	trimethylamine	75	100	300	-	[13]
In	1 at%	acetone	100	300	-	96.8	[14]
Cr	1at%	acetone	500	300	-	~ 92	[15]
Cu	5%	LPG	200	200	1.15	-	[16]
Sn	0.5 at%	LPG	10,000	300	-	88	[17]
Y	1 at%	NO ₂	1	200		~ 90	[18]
Sn	4 at%	ethanol	300	250	150	-	[19]
Mg		H ₂	5000	300	50	-	[20]
In	3 at%	H ₂ S	1000	250	13000	-	[21]
		H ₂			11	-	
		CO			1.5	-	
		LPG			15.8	-	
		ethanol			30	-	
Fe	5 at%	ethanol	1000	27	>70		[22]
In	3 wt%	H ₂	5	300	-	15	This work
		CO				14	
		CH ₄				3	

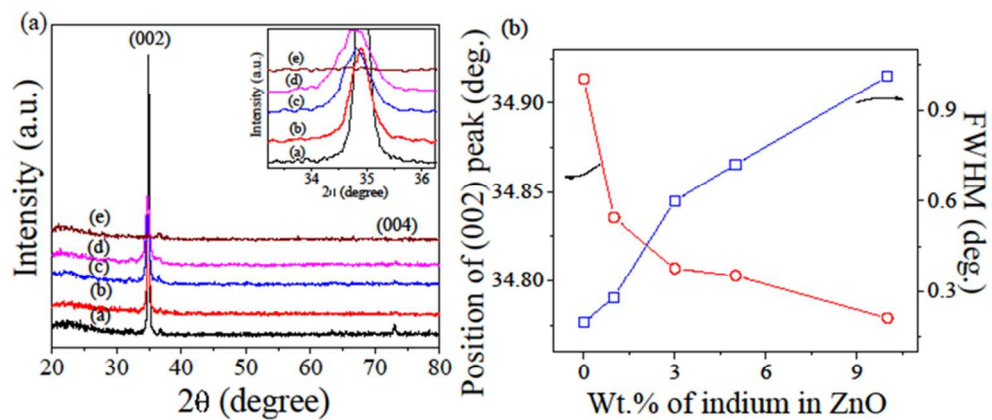


Fig. 1: (a) XRD pattern of (a) undoped ZnO (b) ZnO: In 1 wt% (c) ZnO: In 3 wt% (d) ZnO: In 5 wt%, and (e) ZnO: In 10 wt% thin films. Inset shows the magnified image of (002) peaks of the corresponding films. Fig. 1(b) Position of the (002) peak and full width at half-maxima (FWHM), obtained from the XRD pattern of undoped and indium doped ZnO thin films

Fig.1
254x138mm (96 x 96 DPI)

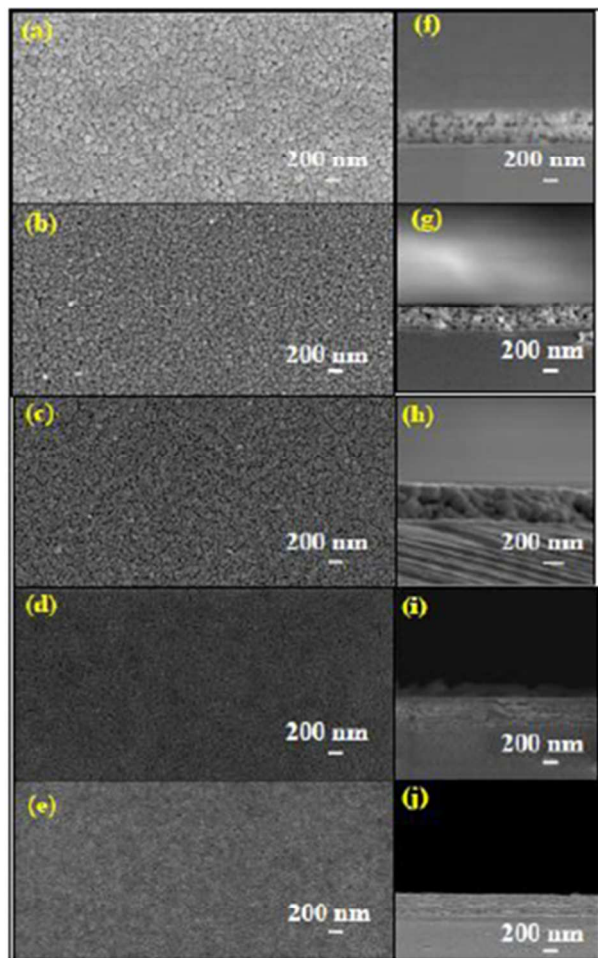


Fig. 2: Scanning electron micrographs of indium doped ZnO thin films of various indium concentration: (a) 0 wt%, (b) 1 wt%, (c) 3 wt%, (d) 5 wt% and (e) 10 wt% and their cross sectional morphology are shown, in the right hand side of the respective films, in Fig. 2f-2j

112x189mm (96 x 96 DPI)

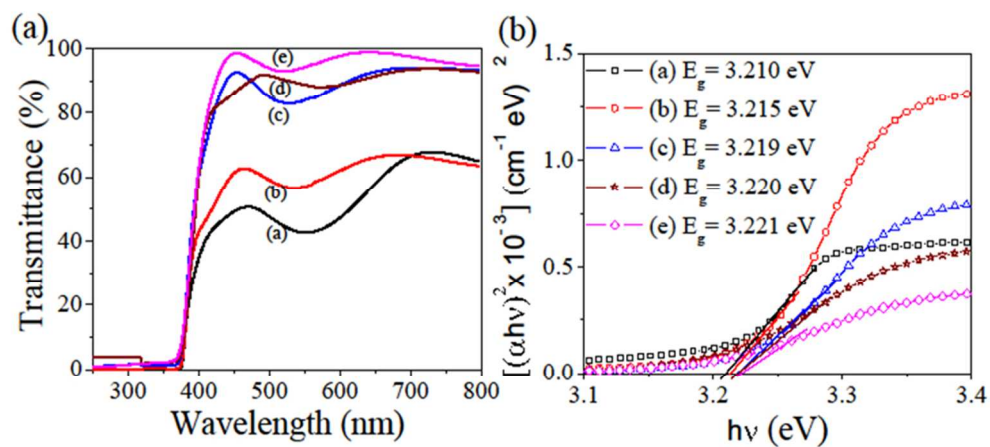


Fig. 3: (a) Transmittance spectra and (b) Tauc plot (showing the band gap of the material) of (a) undoped ZnO, (b) ZnO: In 1 wt%, (c) ZnO: In 3 wt%, (d) ZnO: In 5 wt% and (e) ZnO: In 10 wt% thin films in the wavelength range 250 – 800 nm

254x143mm (96 x 96 DPI)

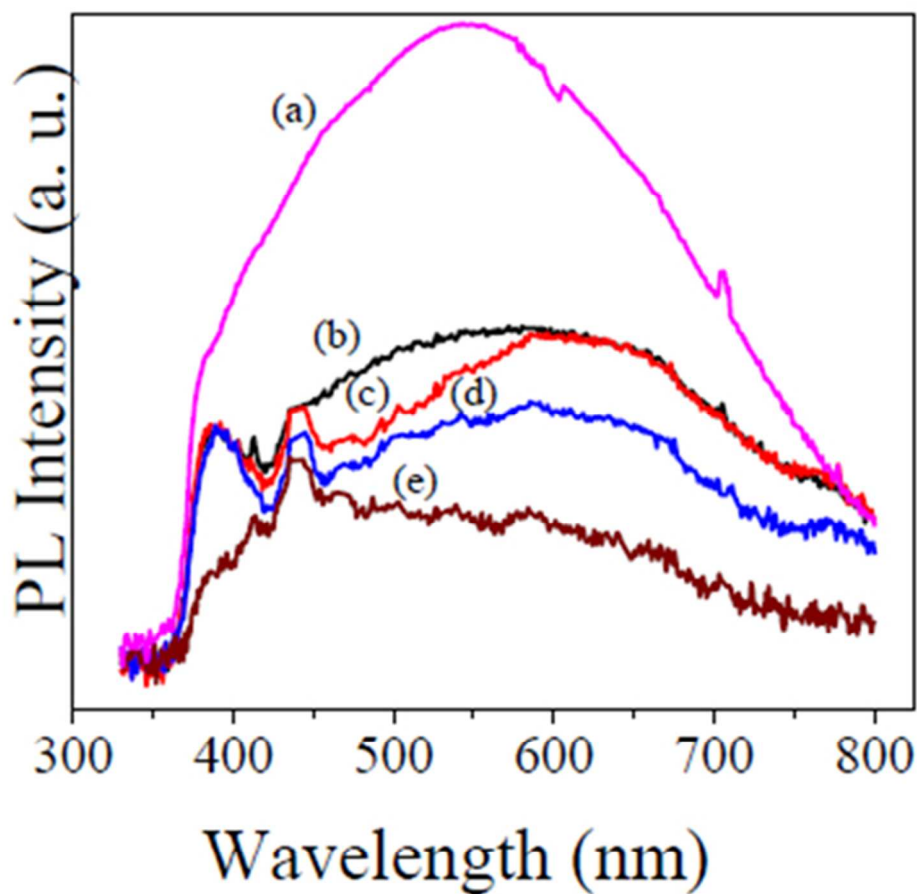


Fig. 4: PL spectra of (a) undoped ZnO, (b) ZnO: In 1 wt%, (c) ZnO: In 3 wt%, (d) ZnO: In 5 wt%, and (e) ZnO: In 10 wt% thin films using He-Cd laser source at an excitation wavelength of 325 nm

153x190mm (96 x 96 DPI)

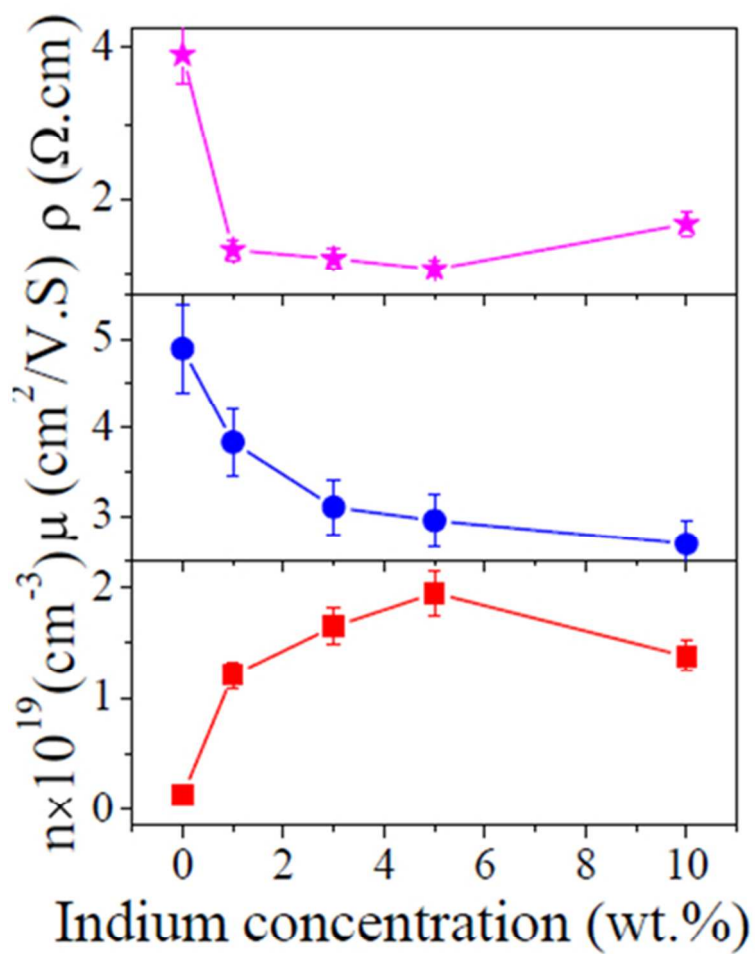


Fig. 5: Plot showing the variation of carrier concentration, mobility and resistivity of the ZnO thin films of various indium concentration at room temperature

123x190mm (96 x 96 DPI)

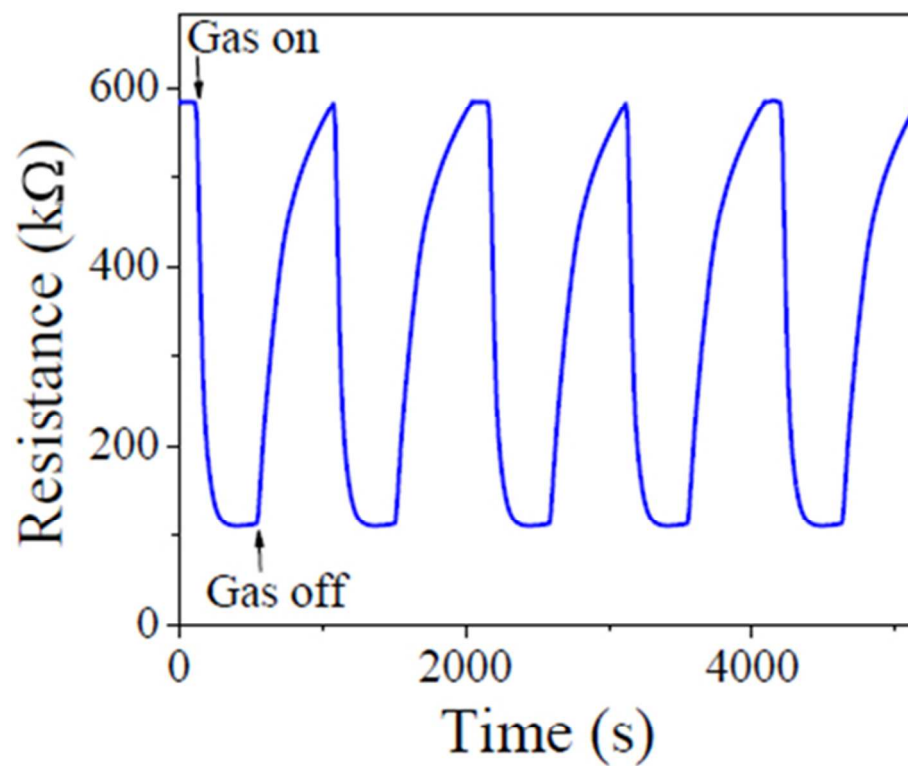


Fig. 6: Resistance transients recorded for 3 wt% indium doped ZnO thin film sensing element towards the detection of 1660 ppm of hydrogen gas at its optimum temperature

154x143mm (96 x 96 DPI)

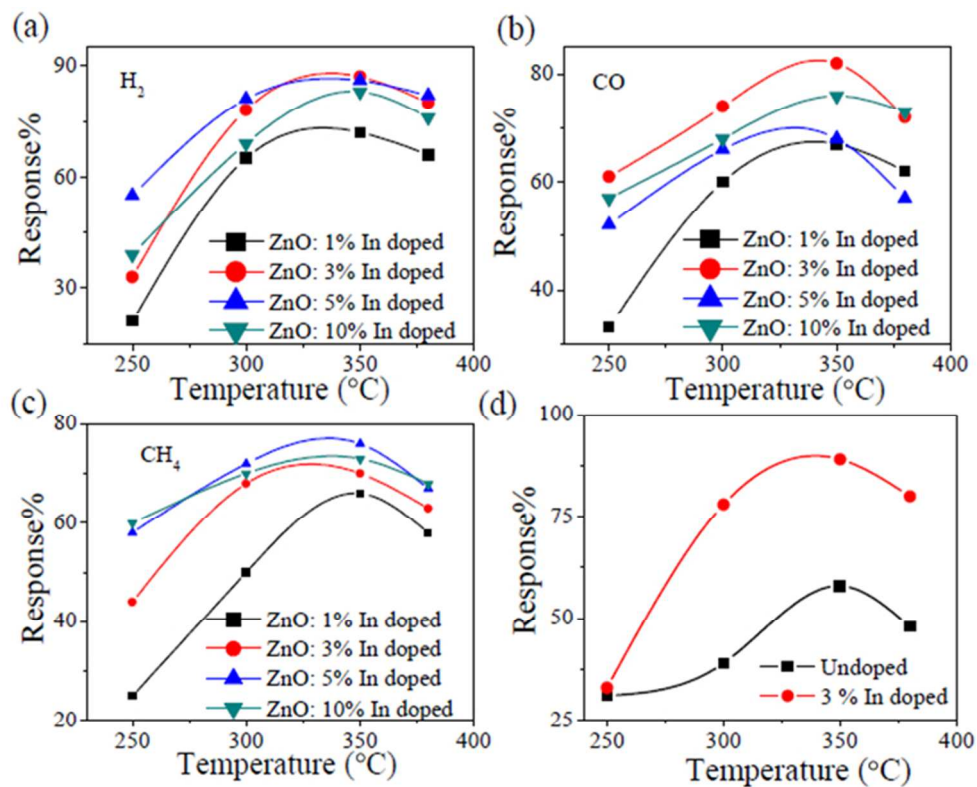


Fig. 7: Variation of response% of ZnO thin film gas sensors (of various indium concentration) towards the detection of 1660 ppm of (a) H_2 , (b) CO and (c) CH_4 gas as a function of operating temperature, (d) Comparison of gas sensing performance of undoped and 3 wt% indium doped ZnO thin film at different operating temperatures

Fig. 7
207x190mm (96 x 96 DPI)

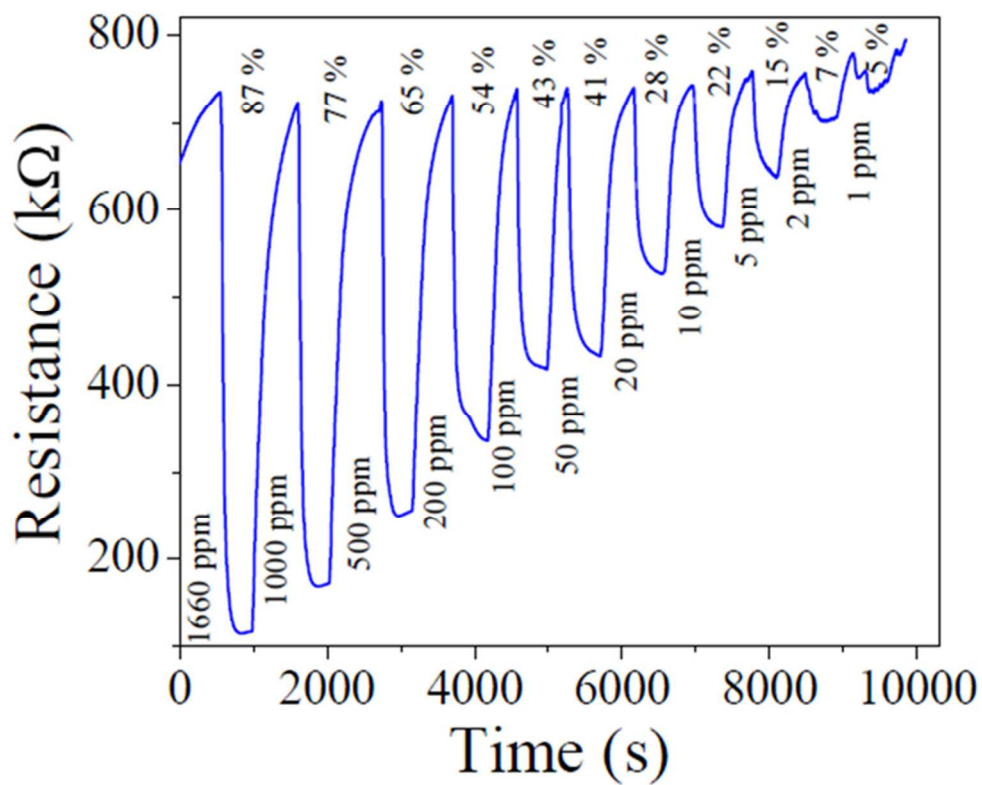


Fig. 8: The time dependent hydrogen gas response of 3 wt% indium doped ZnO thin film gas sensor measured at 350°C, varying the hydrogen concentration in the range of (1660-1) ppm

205x190mm (96 x 96 DPI)

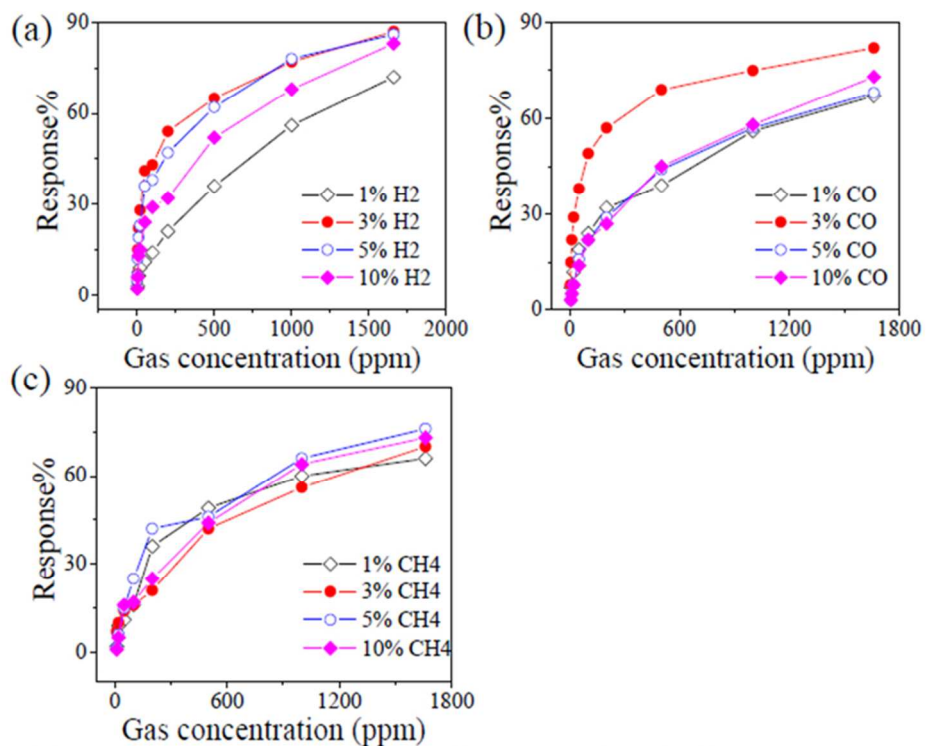


Fig. 9: Variation of response% of indium doped ZnO thin film gas sensors towards the detection of various concentrations of (a) H₂, (b) CO and (c) CH₄ gas at their optimum temperature, 350°C

Fig.9
220x190mm (96 x 96 DPI)